Light Metals 2014
Edited by: John Grandfield
TMS (The Minerals, Metals & Materials Society), 2014

Investigations into Innovative and Sustainable Processes for the Carbothermic Production of Gaseous Aluminum

Efhtymios Balomenos[1], Panagiotis Diamantopoulos[1,2], Dimitrios Gerogiorgis[1], Dimitrios Panias[1], Ioannis Paspaliaris[1], Christoph Kemper[2], Lars Peters[2], Bernd Friedrich[2], Irina Vishnevetsky[3], Michael Epstein[3], Martin Halmann[3], Andreas Haselbacher[4], Zoran Jovanovic[4], Aldo Steinfeld[4]

[1]NTUA (National Technical University of Athens), Laboratory of Metallurgy, Zografos Campus, Athens, 157 80, Greece
[2]IME Process Metallurgy and Metal Recycling, RWTH Aachen University, Intzestrasse 3, Aachen 5206, Germany
[3] Weizmann Institute of Science, POB 26, Rehovot 76100, Israel
[4] ETH Zurich, Sonneggst. 3, Zurich CH-8092, Switzerland

Keywords: Carbothermic reduction of Alumina, Vacuum carbothermic reduction, gaseous Al production, solar furnace

Abstract

Considerable efforts have been applied to produce aluminum by alternative ways. Two novel processes for the carbothermic reduction of alumina towards gaseous aluminum production in Electric Arc Furnace (EAF) and solar furnace have been investigated both theoretically and experimentally. The EAF process was tested at ambient pressures and temperatures above 2500°C in a customized 25 KW hollow electrode EAF, while the vacuum process was preliminary tested at 0.03-2.6 mbar absolute CO partial pressure and temperatures of 1400-1850°C in an induction furnace. Results of both processes confirmed that the full reaction and volatilization of alumina to produce metallic aluminum in the vapor condensers can be achieved only at proper matching of temperatures and pressures at reaction and condensation zones. The solar reactor concept was further explored in a concentrated solar radiation furnace on a 10 kW scale.

Introduction

Current industrial production of aluminum from alumina is based on the electrochemical Hall-Héroult process, which has the drawbacks of high-greenhouse gas emissions, reaching up to 3.82 kg CO_2-equiv/kg Al, and large energy consumption, about 0.056 GJ/kg Al.

A basic non-electrochemical alternative to the Hall-Héroult process is the carbothermic reduction of alumina, which has been proposed by various researchers in the last 50 years [1]. Developed concepts to recover aluminum as liquid metal have encountered significant problems with aluminum carbide formation as well as aluminum vaporization losses. Carbothemic processing of alumina requires high temperatures (> 2100 ^{o}C), where liquid aluminum dissolves up to 20% mol carbon, leading to significant aluminum carbide formation upon cooling. Furthermore at these temperatures extensive aluminum vaporization phenomena occur. A recent thermodynamic study of the system by the authors [2] concludes that aluminum reduction yields are directly related to alumina sub-oxide (Al_2O[g]) vapors formation which is favored when liquid aluminum is in contact with alumina, through the comproportionation reaction:

$$4Al_{[\text{liquid metal}]} + Al_2O_{3[\text{oxycarbide slag}]} = 3Al_2O_{[g]} \quad (1)$$

A way to avoid both problems would be to move the process to conditions favoring gaseous rather than liquid Aluminum production. In this paper two innovative routes towards gaseous carbothermic production are presented.

Vacuum Carbothermic reduction of Alumina

According to the Le Chatelier principle, the extent of a gas producing chemical reaction should be favored by a decrease in the total gas pressure. Thus, under vacuum conditions, the equilibrium of equation

$$Al_2O_{3[s]} + 3C_{[s]} = 2Al_{[g]} + 3CO_{[g]} \quad (2)$$

should be shifted to the right and the onset temperature for the metal production should be significantly lowered [3]. Thermodynamic equilibrium calculations using Factsage software [4] predict the advantage of much lower required reaction onset and completion temperatures for reaction (2), as shown in Figure 1. Similarly the calculated suppression of suboxide vapor production with decreasing overall pressure is shown in Figure 2.

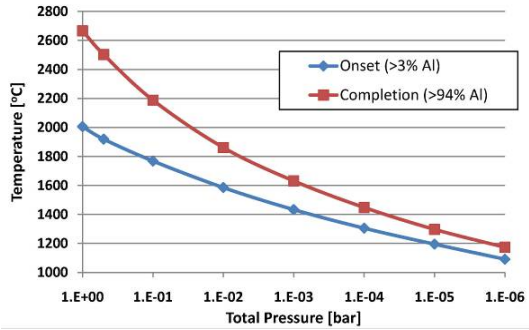

Figure 1. Predicted onset and completion temperatures for reaction (2) under thermodynamic equilibrium at various total pressures. "Onset" is defined here as at least 3% moles (and less than 4%) of Aluminum present as Al[g] and "Completion" as at least 94% moles respectively.

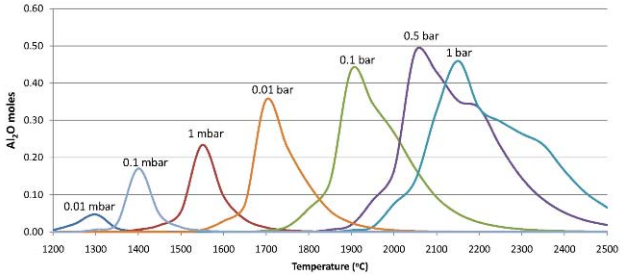

Figure 2. Predicted thermodynamic equilibrium Al_2O(g) moles at various temperatures and total pressures for systems with initial molar composition Al_2O_3+3C.

Experimental validation in inductive furnace

Preliminary experiments in an induction furnace with adjustable till 25kW power at temperatures between 1400-1800 ^{0}C with an argon carrier gas flow and an average CO partial pressure between 0.03mbar to 2.6 mbar, conducted in the Weizmann Institute of Science (WIS), proved the feasibility of the process [3,5]. The forward reaction was fully completed at temperature 1600^{0}C and CO partial pressure 0.2 mbar about, whereas rising CO partial pressure till 2-3 mbar leads to temperature rising till 1800-1850^{0}C. Aluminum yield strongly depends on temperatures of vapor deposit sites to prevent aluminum carbide and oxycarbide formation in backward reactions. The maximum yields were obtained in the region of the condenser where the temperature ranged from 800-850^{0}C. There in the inner layers of the deposits Al yield was as high as 80% whereas in outer surface layers drops of 100% Al were observed. The reason for this is the decreasing CO flow rate and CO partial pressure at the end of the reaction

Furthermore estimation of the energy spent as pumping work reveals, that if the operating pressure is lower than 0.2 mbar then the total estimated energy spent for heating and pumping exceeds the actual energy (which is almost twice the respective theoretical one) spent in the established Hall-Héroult process [3].

For the vacuum process to be sustainable the process heat must be supplied through a renewable source such as through the use of concentrated solar radiation in solar furnaces [3,6] and compromise between temperature and pressure is obligatory to decrease electrical energy consumption for pumping.

Reactor Design

Based on the observations of the induction furnace preliminary experiments and previous experience in solar furnace operation, the main conclusion was creating the reactor with sharp temperature drop from hot zone with temperature suitable for fast kinetic of forward reaction without by product formation and cold zone with deposit sites which temperature is low enough to prevent the backward reaction developing. Design and modeling of solar reactor using FLUENT model were realized at WIS and described in details in [5, 7]. Reactor design and calculated temperature distribution are presented in Figure 3 with highest temperature in reaction zone 1953 K; 320 K in cold zone and the short transition area.

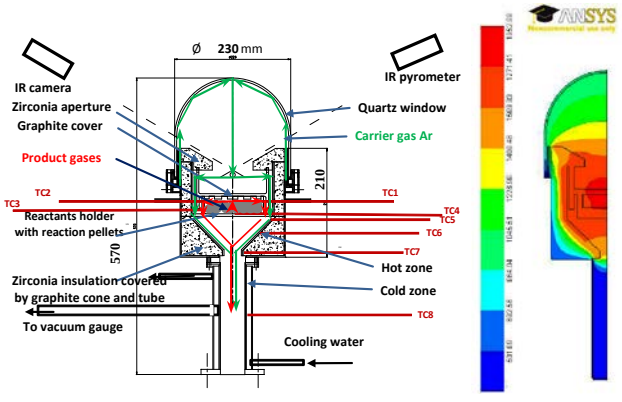

Figure 3. Reactor design (left) and calculated temperature distribution in K, 10.2 kW aperture input (right).

The heat transfer and fluid dynamics in the solar reactor were further analyzed at ETHZ using a coupled Monte-Carlo (MC)/CFD approach. In this approach, radiation is simulated using the ETH Monte-Carlo ray-tracing code VeGaS and the fluid dynamics is simulated with the commercial CFD package CFX in ANSYS 13. The two codes exchange boundary information using a newly developed coupling code that computes boundary condition values based on energy conservation, interpolates as needed, and translates between the different file formats.

The reactor geometry is discretized with 215042 tetrahedral cells. The boundary conditions are solid walls everywhere except for the annular inlet near the bottom of the quartz window through which the Ar purge-gas flows, the outlet, and the crucible bottom, where another inflow boundary is applied. This inflow boundary models the CO produced by the reaction of Al_2O_3 and C. Thus the reactants and their particulate nature are not directly simulated. The mass flow rate is determined by assuming that 10% of the radiative flux absorbed by the crucible covers is used by the reaction.[1] It is assumed that the Ar purge gas is supplied at the same mass flow rate and that it enters the dome at a temperature of 300 K. At the outlet, a pressure of 10 mbar is imposed, which is significantly higher than the real outlet pressure. In the simulations, convection heat transfer is neglected because of the low pressures in the reactor and, as a first approximation,the conduction heat flux is taken to be 20% of the radiative flux absorbed by the crucible cover. The total irradiation power is 10^4 suns. In the MC simulations, 2×10^7 rays were used, chosen as a compromise between statistical independence and required computation time. All solid walls are assumed grey and diffuse.

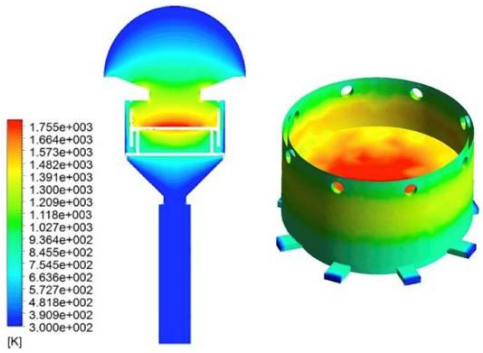

Figure 4. Fluid temperature contours on a cross-section through the reactor (left) and temperature contours on the crucible and crucible cover (right).

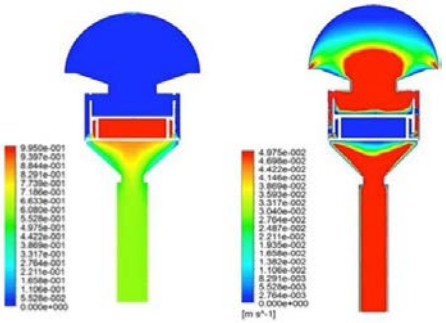

[1]The 10% is a conservative estimate for the overall solar energy conversion efficiency from solar-to-reaction enthalpy, taking into account optical losses of solar concentration, solar reactor losses of heat transfer, and irreversibility losses of the chemical transformation. Ongoing research with simulations of higher fidelity may eventually provide more accurate estimates that could be used in future work.

Figure 5. CO volume fraction (left) and Ar velocity (right) on cross-section through the reactor.

The fluid temperature contours on a cross-section through the reactor and on the crucible and crucible cover are shown in Figure 4. The highest temperatures of about 1800 K near the crucible cover can be seen clearly. The figure also shows how the simulation allows resolving small-scale features of the geometry like the crucible supports. The temperature on the crucible cover exhibits a significant radial gradient. In Figure 5, the volume fraction of CO and velocity of Ar are shown on a cross-section through the reactor. The simulated production of CO in the crucible is clearly visible including the subsequent mixing with Ar and its transport downstream through the cold zone. The Ar velocity is high near the annular inlet and the aperture as well as when it flows past the crucible into the cold zone.

Experiments in solar furnace

In order to reach a reaction temperature above 1600°C, the optical facility with high concentration (~5000 suns) available at the Weizmann Solar Tower was exploited to power the concentrated solar radiation furnace reactor.

The principal optical scheme of the solar furnace used is presented in Figure 6: a heliostat reflects solar energy on the concentrating parabolic dish through intermediate flat mirror. Concentrated solar light enters the reactor (Figure 7) first through a spherically shaped quartz window that can withstand the internal vacuum conditions and then through zirconia aperture placed at the focal plan of the dish.

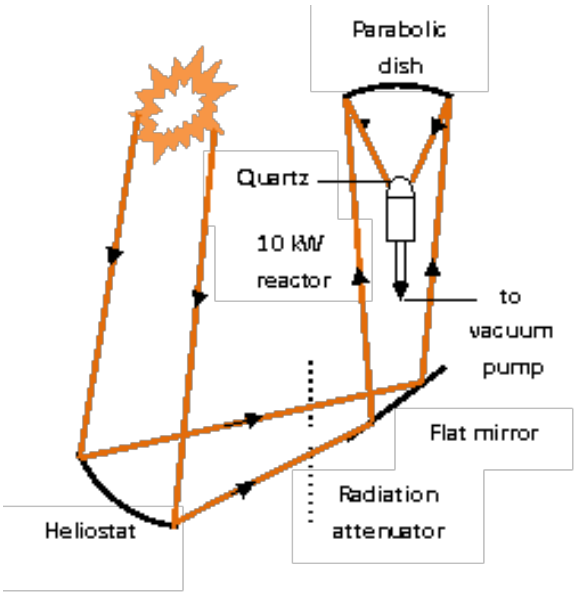

Figure 6: The principal optical scheme of the solar furnace

The reactor itself (Figures 3, 7) contains a graphite crucible with cover to prevent product vapors released from the reactant holder from settling on the quartz window, a graphite cone that serves as part of the hot zone, and a water-cooled stainless steel tube (0.05 m diameter) that functions as the main cold deposit site for aluminum vapors. The exit of the reactor is connected with a dry vacuum system: model DRS1 made by Alcatel, comprising of ACP40 multi-stage Roots pump operating without internal lubricant and Roots blower RSV301B with bypass capable of 250 m3/h peak pumping speed with 1000 mbar maximal continuous inlet pressure and 0.003mbar ultimate pressure. The DRS1 is equipped with a filter and a liquid nitrogen trap at its entrance. Vacuum is measured by two convection vacuum gauges (Model CVM-211 by Instrutech Inc), ones placed at the cooling tube of the reactor, where the pressure is lower than the pressure in the hot reaction zone, and the other at the entrance to the pumping system.

Flow rate at the exit of the reactor is measured by flow meter that was connected with the outlet of the DRS1. Input of carrier gas 1l/min was supported by flow controller and inlet and outlet pressures were measured by pressure transmitters. Temperature of quartz window was observed by IR pyrometer, while the temperatures in solar reactor are measured by 8 thermocouples type C suitable for high temperature W-Re (tungsten-rhenium) (XMO-W5R26-U-125-30-H-HX-18 by Omega) placed in different locations of the hot and cold zones.

The graphite crucible was loaded with pellets prepared using wood charcoal as biomass source and 10 μm alumina powder by Sigma Aldrich and also metallurgical alumina powder by AoG (Aluminion S.A. plant in Greece) at stoichiometric reaction mixtures. 10 wt.% sugar powder was used as a binder. The mixture were pressed in the special holder under 10 tons and subsequently heated to 165°C for 20 min. Sugar powder as a binder was selected as a pure thin sticky powder with a known formula and a low melting point.

During operation of the furnace Ar is used as a carrier gas, which along with the gases exiting the graphite crucible, is evacuated through the filters and nitrogen trap by the dry vacuum system. The exhausted gases are analyzed by Siemens infrared analyzer Ultramat 23 calibrated to CO, CO_2 and O_2. Absence of O_2 in the output gases confirms the absence of leaks in the reactor

Figure 7. Solar reactor in operation (left) and cooling afrer operation (right)

Mass balance of the carbothermic reduction reaction was estimated through the oxygen yield as number of moles of CO in the output gases (as measured through infrared analyzer) divided by the number of oxygen atoms in the reacted alumina [moles CO /(3*moles reacted Al_2O_3)]. Metallic Aluminum yield was estimated as total weight of pure aluminum in deposits (as measured though quantitative XRD analysis of collected deposits) divided by the weight of aluminum in the reacted pellets.

Main results of the tests that were made at different weather and temperature conditions and CO partial pressure are presented in Tables I and II.

Samples with a significant amount of pure aluminum were deposited at the exit of the graphite cone on a sub-layer of carbide, on the internal surface of the water cooled tube, and in the filters. Aluminum carbide and oxycarbide were formed both on hot sites as products of carbonization of deposited Al when temperatures were not high enough to prevent the deposition, and in the sample holder as by-products of the forward reaction during the initial preheating and when reaction temperature was not high enough. Certain amount of alumina was also observed in the cold zone that could be formed during deposition of volatile suboxide as backward reaction presented by Eq. (1).

Table I. Experimental Results of Solar testing

Test No	Avg. DNI (Direct Normal Irradiance)	Avg reaction temp [^{o}C]	Avg. CO partial pressure in the cooling tube area P_{CO}[mbar]	Oxygen yield [%]	Al yield (weight conversion) [%]
1	924*	1525	0.04	93	90
2	812**	1442	0.07	79	30
3	744***	1486	0.17	78	44
4	903*	1579	0.31	---	---
5	860*	1548	0.19	76	34
6	858*	1528	0.06	91	74

*no clouds, ** clouds during 20% of the reaction time, *** clouds during 9% of the reaction time

Table II. Experimental Results and quantitative XRD analysis

Test No	Mass of Al in reacted pellets [g]	Hot Zone deposit weight [g] / wt% Al	Cold Zone deposit weight [g] / wt% Al	Filters deposit weight [g] / wt% Al
1	2.68	0.53g / 70.3% Al	1.75g / 89%Al	0.47g / 91%Al
2	6.86	2.02g / 8.8% Al	3.84g / 27.2% Al	0.62g / 2.7% Al
3	7.25	2.11g / 7.5% Al	3.97g /56.6% Al	0.71g / 33.5%Al
4	11.13	3.38g / 28.1% Al	6.6g / 42.3% Al	1.41g / 3.1%Al
5	9.87	2.46g / 22%Al	6.0 g / 54.6% Al	2.57g / 0.0% Al
6	6.80	1.87g / 29%Al	5.33 g / 92.7% Al	1.74 g / 50.0% Al

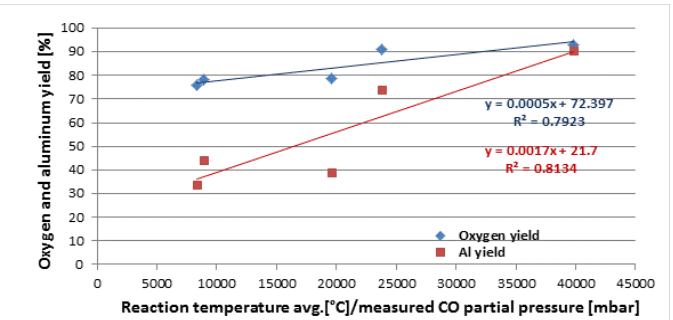

Figure 8. Observed oxygen and aluminum yields as a function of the measured average reaction temperature to the respective measured CO partial pressure.

From the results in the tables above it is possible to conclude that the reduction of alumina and the production of metallic Aluminum decreases with the decreasing of the temperature and the increase of the CO partial pressure in the reactor, as shown graphically in Figure 8. In Figure 8 it can also be marked that aluminum yield is usually less than oxygen yield because of carbide formation.

High Temperature Gaseous Al Production

As seen in Figure 1, for the system Al_2O_3 + 3C at atmospheric pressures it is thermodynamically possible to achieve high gaseous aluminum reduction yields at temperatures above 2600^{o}C. Such temperatures can be reached in plasma reactors and DC Electric Arc furnaces. In the DC EAF an electric arc can be produced and sustained between the bottom and top electrode. In the absence of a liquid melt which would act as current conductor, the transformation of electric energy to heat takes place through the ionized plasma of the arc, in which the temperatures may reach up to 6000 ◦C [8]. Using a hollow top electrode (or a lance feeder) the material can be fed directly into the arc zone at controlled rates. This allows to feed alumina-carbon pellets "one-at a time" in order to volatilize them, while avoiding the creation of a liquid phase, as seen in photograph presented in Figure 9.

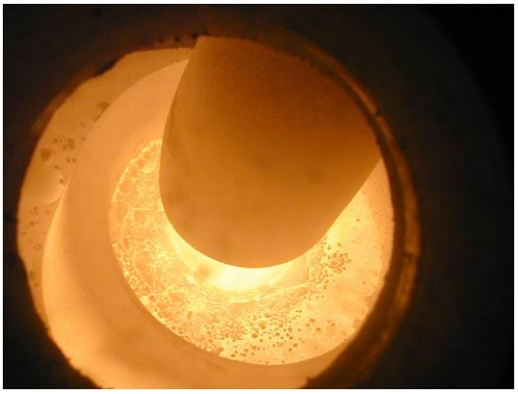

Figure 9.Photo of the hollow DC-EAF in operation. The alumina-charcoal pellets are fed through the top electrode directly into the arc zone between electrode and crucible bottom. The pellets vaporize almost immediately leaving no liquid phase.

Once the aluminum has been reduced to vapors, as discussed in the previous section the key issue is to achieve fast condensation minimizing back reactions with CO gases.

Experimental Setup and Equipment Optimization

To test this process a custom hollow electrode DC-EAF, depicted in Figure 10, located at IME, RWTH Aachen was used. The top electrode was a hollow electrode, made by graphite, with outer diameter 50mm and inner 30mm, properly connected via a flange with a feeding system. The later had an automated rotary system to control the feeding rate of the pellets into the reactor and an argon carrier gas feed to ensure that no product off gasses would enter the hollow electrode. The lid of the furnace was water-cooled and was connected to a strong off-gas suction system. Inside the furnace a graphite crucible with an inner diameter of 120 mm was placed on top of the bottom electrode with a fine bed of coke grains in between them to ensure maximum conductivity and practically transform the bottom of the crucible to the bottom

electrode of the EAF. Additional argon feeds where available through the coke bed and the furnace lid. Furnace insulation consisted of a cylindrical graphite felt (58 mm thick), followed by a thicker outer alumina blanket (110 mm thick).
The water cooled lid of the furnace was fitted with a custom designed copper condenser through which the off gases exit the furnace and entered the universities off-gas handling system. The geometry of the condenser was designed based on CFD simulations in order to achieve within the condenser homogenous laminar flow with a minimum overall layer thickness. This was based on the notation of maximizing the volume off-gases directly in contact with the condenser walls and thus allowing maximum Aluminum condensation. To this end rectangular fins were added to the walls of the cylindrical condenser along with a V shaped fin at the entrance of the off-gasses. The geometry of all of the above components was optimized through CFD modeling using COMSOL Multiphysics software. The optimal result of the simulation is shown in Figure 11.

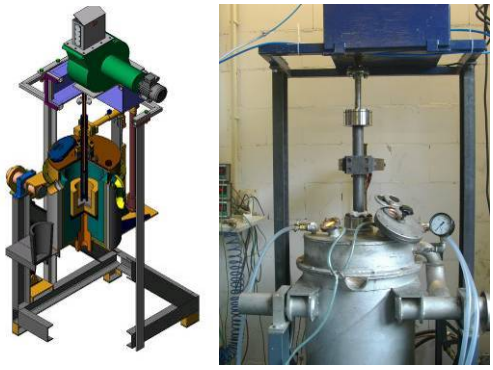

Figure 10. 3D model and actual photo of the hollow electrode EAF with automated feeder which was used in the experiments

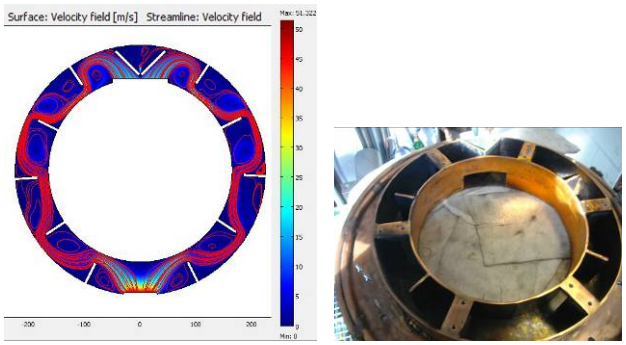

Figure 11. Left: CFD modeling of the gasses velocity field in the condenser. Right: Actual photo of the inside of the copper condenser build.

Experimental procedure

Using the above described equipment an experimental campaign took place in order to optimize operating conditions such as pellet feeding rate, Ar carrier flow rates, off-gas suction and others in order to attain metallic Aluminum deposits in the condenser.
All experiments were conducted with reaction stoichiometric pellets made from metallurgical alumina supplied by AoG and wood charcoal. As binding agent corn starch was used and the pellets were cured at 160^{o}C for 16 h.
Prior to each experiment the furnace was preheated for 20 min with resistance heating (the top electrode in contact with the crucible bottom) and for another 20 min with arc radiation heating (the top electrode a few cm above the crucible bottom). Then the pellets were fed in the reactor at rates between 1 to 3 gr/min for 20 to 30 min. After the end of the experiment the furnace was allowed to cool under protective atmosphere for 1hour and then the condensate from the condenser was collected and analyzed through quantitative XRD analysis and SEM.

Experimental results

Initial tests with the copper condenser produced condensates containing up 44% metallic aluminum, up to 21% Aluminum carbides and oxycarbides and the remaining as alumina both as corundum and as cubic alumina (see Figure 12). Given that the alumina used in the pellets was gamma alumina (rhombohedral structure), the cubic structure alumina found in the condensate must be attributed to re-oxidation of condensed metallic aluminum after the end of the experiment, at low temperatures. This hypothesis was verified through SEM examination of the collected powders, which revealed a material with a "wool" like microstructure, completely different from the microstructure of the initial pellets used (Figure 13). SEM-EDS analysis of the "wool" reveals 61%wt Al and 39%wt O. Given that the composition of alumina is 52%wt Al and 47%wt O, one can deduce that the "wool" was condensed as nano-size metallic aluminum powder and after the experiment, upon contact with air, underwent intense surface oxidation.

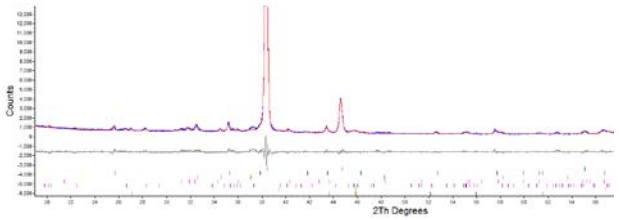

Figure 12. XRD analysis of the dust collected from the condenser. Both major picks correspond to metallic aluminium (2theta 38,10 and 44.37). Rietveld-method analysis shows at least 44% metallic Al, followed by 20% cubic Alumina, 15% Corundum, 8% Al_2OC, 7% Al_4C_3 and 6% Al_4O_4.

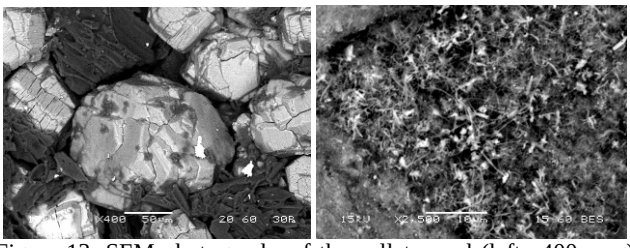

Figure 13: SEM photographs of the pellets used (left x400 mag) and of the powder collected in the condenser after the experiment (right).

To further improve the process it was assumed that higher cooling rates where needed in the condenser, which was water-cooled only at its basis. Therefore dry and regular ice were used to cool the external surface of the condenser during the experiment. This resulted indeed in minimization of back reactions with carbon monoxide as the powder collected and analyzed with XRD (Figure 14) contained 77% metallic Al, 9% cubic alumina and less than 14% in all other phases.

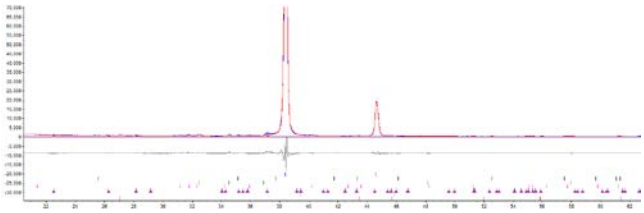

Figure 14. XRD analysis of the powder collected from the condenser. Both major picks correspond to metallic aluminium (2theta 38,10 and 44.37). Rietveld-method analysis shows at least 76.91% metallic Al, followed by 9.37% cubic Alumina and 4% or less in Al_2OC, Al_4C_3 and Al_4O_4C.

Quantitatively, in this optimum experiment, 30 g of material pellets were consumed and at end of the experiment 16 g of dusty material were retrieved from the condenser. For reaction stoichiometric composition the 30 g of pellets would contain 11.7 g of Al, 10.4 g of O and 7.8g of C. According to the quantitative XRD analysis presented above the powdered deposits contained 7.1 g of metallic Aluminum, thus achieving a 61% metallic aluminum recovery yield. The other phases present in the powder contained 5.4 g of Al. In total the powder seems to contain 12.5 g of Al, i.e. 0.8 g more than the initial amount of Al. Of course given that the results are based on quantative XRD analysis, the error here is within reason.

These first results prove that the process is feasible and with a more optimized reactor design, potentially complete metallic aluminum recovery could be achieved. Key to the process is the condenser which has to be radically re-designed so as to achieve maximum cooling rates with short off-gas retention times.

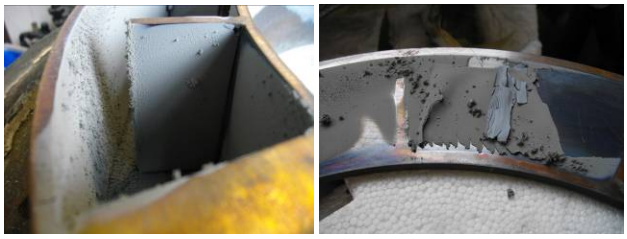

Figure 15: Powdered "metallic" material collected at the copper condenser after the experiment.

Conclusions

Two seemingly completely different approaches towards carbothermic reduction of alumina have been presented. Both are motivated by the potential of producing gaseous rather than liquid aluminum without formation of aluminum carbides and encountering product vaporization losses.

The vacuum carbothermic reduction process, supplies part of the required energy as pumping work and utilizes concentrated solar radiation for the remaining part. Thus the potential of using solar energy to produce aluminum via carbothermal reduction of alumina under vacuum has been demonstrated. The investigations to follow relate to the creation of a feeder reactor, in order to realize preheating with an empty sample holder and thus prevent by-product formation during this initial phase.

The high temperature process achieves also the production of gaseous Al relying on industrial mature technology. While this was tested in lab scale DC-EAF, it is obvious that the process would also work in modern day plasma reactor, where higher material outputs and better atmosphere control can be achieved.

On the other hand both processes have to combat the difficult issue of condensating the Al vapors without back-reactions with carbon-monoxide. This is clearly an issue of reactor design as the condenser geometry and cooling rate have to be optimized in regards to the process's off-gasses output. The complete avoidance of carbide formation might not be possible, but small amount of Al-carbides can be easily removed and recycled in the process through a simple melt refining step, as carbon solubility in liquid aluminum at temperatures below 1000 ^{0}C is practically zero.

For either process extensive research is needed in alternative gas quenching processes like supersonic quenching or quenching in liquid metal baths, in order to produce a potentially industrially applicable process with continuous Aluminum metal production. The ideal goal would be to achieve gas condensation to liquid metal aluminum at temperatures around 800 ^{0}C thus allowing continuous metal removal and avoiding the al-carbide refining step.

Investigations into a hybrid (electric-solar) reactor and different condenser design, which would allow even for liquid aluminum recovery, are the next steps in the research efforts of the authors.

Acknowledgements

The research leading to these results has received funding from the European Union Seventh Framework Programme ([FP7/2007-2013]) under grant agreement n° ENER/FP7/249710/ENEXAL (www.labmet.ntua.gr/ENEXAL)

References

1. B.J. Welch, Aluminum Production Paths in the New Millennium, *JOM*,51(5) (1999), 24-28

2. E. Balomenos et al., Theoretical Investigation of the Volatilization Phenomena Occurring in the Carbothermic Reduction of Alumina, *World of Metallurgy – ERZMETALL*, 64(6) (2011), 312-320.

3. M. Halmann et al., Vacuum carbothermic reduction of alumina, *Mineral Processing & Extractive Metall. Rev.*, 35 (2014) 126–135.

4. C.W Bale et al., "FactSage Thermochemical Software and Databases", Calphad 26(2) (2002), 189-226

5. I.Vishnevetsky et al., Solar carboreduction of alumina under vacuum, JOM, Materials and Processes for Renewable Energy, special issue, December 2013, in press.

6. E. Balomenos et al., Exergy Analysis of Metal Oxide Carbothemic Reduction under Vacuum – Sustainability prospects, *IJoT*, 15 (3) (2012), 141-148.

7. R. Ben-Zvi, Numerical simulation and experimental validation of a solar metal oxide reduction system under vacuum, accepted by *Solar Energy*, Ref.No.:SE-D-13-00762R2.

8. G. Bellussi et al., eds,. Ullmann's Encyclopedia of Industrial Chemistry, "*Metallurgical Furnaces*"(John Wiley and Sons, Inc., 1999-2013,Online ISBN: 9783527306732, DOI: 10.1002/14356007)

Light Metals 2014
Edited by: John Grandfield
TMS (The Minerals, Metals & Materials Society), 2014

A CFD-PBM COUPLED MODEL PREDICTING ANODIC BUBBLE SIZE DISTRIBUTION IN ALUMINUM REDUCTION CELLS

Shuiqing Zhan[1], Mao Li[1,2], Jiemin Zhou[1], Jianhong Yang[3], Yiwen Zhou[3], Chenn Q Zhou[2],
[1]School of Energy Science and Engineering, Central South University, Changsha 410083, Hunan, China;
[2]Center for Innovation through Visualization and Simulation, Purdue University Calumet, Hammond, IN46323, USA;
[3]Zhengzhou Research Institute, CHALCO Ltd, Zhengzhou 450041, Henan, China

Keywords: aluminum reduction cells, multiphase flow, population balance model, bubble size distribution

Abstract

In order to understand more details of anodic bubble formation, coalescence and movement mechanism under the horizontal anode bottom, a population balance model (PBM) was used to calculate the anodic bubble size distribution (BSD) in aluminum reduction cells. The proposed PBM was numerically solved with a class method (CM) which has been provided in ANSYS FLUENT. A CFD-PBM coupled model that combines the PBM and CFD model was used to simulate more complex flow behavior with proper coalescence and breakage mechanism of anodic bubble. A modified k-ε turbulence model was used to describe liquid phase turbulence in the simulation. The effects of current density, anode width and the presence of slots on the BSD have been investigated. In addition, the relative influence of the bath flow induced by the cell magneto-hydrodynamic (MHD) on the BSD is also discussed. The predicted BSD is in accordance with a series of literature experimental results.

Introduction

During the operation of commercial aluminum reduction cells, anodic bubble (mainly carbon dioxide) is generated under the anode bottom, and move up through the bath under the influence of buoyancy, recirculation flows. The anodic bubble induces bath flow in the cell which plays an important positive role in homogenization of the alumina distribution and temperature field. Due to the large area of the anode, the anodic bubbles gradually gather under the anode bottom, therefore, the phenomenon of coalescence and breakage can often occur between bubbles, which can produce some bubble group with different sizes, forming a certain thickness of the bubble layer. Conversely, the bubbles increase voltage drop under the anode bottom which in turn results in high energy consumption during the electrolytic process.

The previous studies of anodic bubble distribution characteristics are mainly focused on three aspects: the physical modeling, electrolytic test and numerical simulation. Fortin et al. [1] was the first to use a full-scale water model to study the effects of some key operating parameters i.e., current density, anode-cathode distance and anode inclination angle on the bubble layer, anode bubble coverage and bubble release frequency. Solheim et al. [2] found that bubble size decreased with the addition of propanol which inhibits the coalescence. It was reported that the small bubble results in high accumulated gas volume as well as high resistivity in the bubble layer. Xiang-peng L et al. [3] reported that bubble size increased with an increase in liquid surface tension and decreased at high anode inclination angle. Qian and Chen [4-6] presented a comprehensive review of the phenomenon of bubble formation, coalescence, breakage and movement mechanism under the horizontal anode bottom and found that there was a strong relationship between the anodic bubble size distribution and anode material, spatial position(anode bottom or side channel) and the operation parameters.

In summary, it is clear that the initial bubbles generated under the anode bottom are very small and generally uniform in size. The existence of these small and uniform bubbles can form more and more large bubbles, which have an important influence on the electrolysis process. Physical modeling using the compressed air as the anode gas is not perfect due to restriction on experimental condition, where the mechanism of the generated gas is different from electrochemical reaction. On the other hand, the spatial bubble size distribution of electrolytic test system dose not apply to real industrial aluminum reduction cells because of small scale of the model (10-20mm) as compared with that of the real cells. Although there have already been more and more studies on the experiments, a lot of key problems are still remaining unsolved. Neither small scale electrolysis test nor real scale water-air model can reproduce correctly the morphology and the dynamics of the bubble size distribution in aluminum reduction cells.

Many numerical simulations based on the prediction of complex gas-liquid flows were also used to study aluminum reduction cells system with different focuses. There are several methods available for the mathematical modeling of two-or multiphase flow, i.e., the volume of fluid (VOF) method, the Euler-Euler method and Euler-Lagrange method [7-10]. To some extent, these methods could predict the multiphase flow field and the bubble volume fraction or size distribution based on constant bubble size modeling, but could not obtain real bubble size distribution. Owing to the fundamental importance of bubble size in anodic bubble-bath flows, the predictions of bubble size distribution become very important for the understanding of the hydrodynamics of aluminum reduction cells. Moreover, the bubble size under the anode bottom is dependent on local turbulence intensities as they directly affect the bubble coalescence and breakage phenomena.

In recent years, there have been a number of studies [11-14] using population balance model(PBM) to calculate the distribution of bubbles with gas-liquid two-phase Euler-Euler model by considering bubble coalescence and breakage phenomena. At present, the most widely used in industry is bubble columns, where many valuable conclusions have been provided. To date, however, we have yet to see any studies on taking into account the coalescence and breakage of anodic bubbles in aluminum reduction cells. We have used a two-fluid Euler-Euler model with constant bubble size for the calculation of interfacial forces in the governing equations of CFD previously [15]. In the present work, a CFD-PBM coupled model that combines the PBM and CFD model was used to simulate more complex anodic bubble/bath